have to travel normal to the layer structure. The film thickness must be sufficiently small to keep the contact resistance low (Fig. 3B).
15. M. Shur, M. Hack, J. G. Shaw, *J. Appl. Phys.* **66**, 3371 (1989); M. Shur and M. Hack, *ibid.* **55**, 3831 (1984).
16. G. Horowitz and P. Delannoy, *ibid.* **70**, 469 (1991).
17. K. D. Mackenzie, A. J. Snell, I. French, P. G. Le Comber, W. E. Spear, *Appl. Phys. A* **31**, 87 (1983); A. C. Hourd and W. E. Spear, *Philos. Mag. B* **51**, L13 (1984).
18. This is not the result of an increase of V_0 (Fig. 3A) shifting only slightly from $V_0 \approx 3$ V at 320 K to $V_0 \approx -2.5$ V at 144 K.
19. It was assumed that V_0, which is read directly from the transfer characteristics, can be taken as a rough estimate for V_{FB}, that is, $n^S_{ind} \approx C_i/e(V_g - V_0)$.
20. L. Torsi, A. Dodabalapur, L. J. Rothberg, A. W. P. Fung, H. E. Katz, *Science* **272**, 1462 (1996).
21. ———, *Phys. Rev. B* **57**, 2271 (1998).
22. A. Dodabalapur *et al.*, *Appl. Phys. Lett.*, in press.
23. We thank B. K. Papworth for the photograph, P. Brown and M. Matters for discussions, I. Musa for growing the SiO_2 gate oxide, and Cambridge Display Technology for the MEH-PPV polymer. Supported by the European Commission (ESPRIT 24793–Frequent) and the Engineering and Physical Sciences Research Council.

16 March 1998; accepted 23 April 1998

Carbon Nanotube Quantum Resistors

Stefan Frank, Philippe Poncharal, Z. L. Wang, Walt A. de Heer*

The conductance of multiwalled carbon nanotubes (MWNTs) was found to be quantized. The experimental method involved measuring the conductance of nanotubes by replacing the tip of a scanning probe microscope with a nanotube fiber, which could be lowered into a liquid metal to establish a gentle electrical contact with a nanotube at the tip of the fiber. The conductance of arc-produced MWNTs is one unit of the conductance quantum $G_0 = 2e^2/h = (12.9 \text{ kilohms})^{-1}$. The nanotubes conduct current ballistically and do not dissipate heat. The nanotubes, which are typically 15 nanometers wide and 4 micrometers long, are several orders of magnitude greater in size and stability than other typical room-temperature quantum conductors. Extremely high stable current densities, $J > 10^7$ amperes per square centimeter, have been attained.

The intriguing possibility that nanoscopic graphitic structures may someday be used as electronic elements has been reinforced by predictions (*1*) as well as recent demonstrations (*2–4*) of their device properties. However, not much is known about the electronic transport in nanotubes. Theory predicts that the electrons flow ballistically through them and that the conductance (the inverse of the resistance) is quantized (*5–7*), but neither effect has been observed previously (*3, 4, 8–13*).

Quantized conductance results from the electronic wave guide properties of extremely fine wires and constrictions [see, for example, (*13–20*)]. When the length of the conductor is smaller than the electronic mean free path, then the electronic transport is ballistic, in which case each transverse wave guide mode or conducting channel contributes G_0 to the total conductance. Calculations indicate that conducting single-shell nanotubes have two conductance channels (*5–7*). This predicts that the conductance of a single-wall nanotube (SWNT) is $2G_0$ independent of diameter and length.

Another important aspect of ballistic transport is that no energy is dissipated in the conductor (*20*). Instead, the Joule heat is dissipated in the electrical leads, which connect the ballistic conductor to the macroscopic elements of the circuit. The nondissipative property survives if elastic scattering occurs, for example, from impurities and defects. However, elastic scattering affects the transmission coefficients and thereby reduces the conductance (*20–22*), which then is no longer precisely quantized [see (*19*)].

Until recently, conductance quantization had only been observed in two-dimensional electron gases at ultralow temperatures (*15*). Room-temperature quantized conductance has now also been observed in metallic wires, which usually are at most a few nanometers long and a fraction of a nanometer wide (*16–19*). Although conductance quantization requires ballistic transport (*20–22*), we were able to demonstrate both properties independently.

In our experimental scheme we used arc-produced multiwalled carbon nanotubes (MWNTs) (*23–26*). The nanotubes were typically very straight with lengths of 1 to 10 μm (*24, 25*) (Fig. 1). High-resolution transmission electron microscopy (HRTEM) showed that their diameters ranged from 5 to 25 nm, with inner cavities from 1 to 4 nm; they typically had about 15 layers (*25*). The nanotubes were embedded in fibers that occur in the soft material inside the hard-shelled deposit of the arc (*24, 25*). These fibers are very fine and compact (nominally 50 μm in diameter at the tips and 1 mm long) and are composed of nanotubes and graphitic particles; TEM revealed that usually several particularly long (>3 μm) nanotubes protrude from the tip of the fiber. The protruding nanotubes are usually bundled with others of different lengths, hence only one nanotube is at the extreme end. An example is shown in Fig. 1. The nanotube fiber was attached to a gold wire with colloidal silver paint, and the resulting nanotube contact was installed in place of the tip of a scanning probe microscope (SPM) (*27*) so that the nanotube contact could be raised and lowered using the SPM controls. A heatable copper reservoir containing mercury (or other low–melting temperature metal) was placed below the nanotube contact. The liquid metal was used as the second contact to the nanotubes and allows a gentle and reproducible contact with the nanotubes to be made (mercury does not wet the nanotubes). Moreover, TEM revealed that before the nanotubes are dipped in the liquid metal, they are covered with fine graphitic particles. Dipping them had a cleansing effect, and afterward the protruding

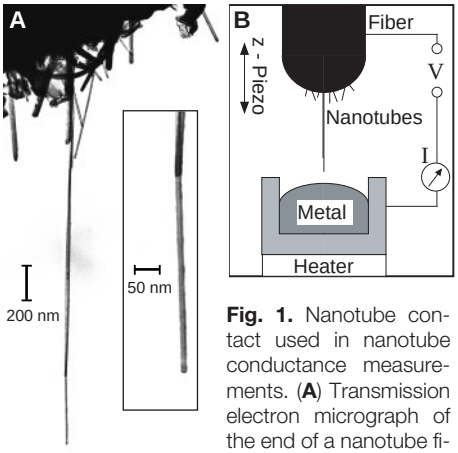

Fig. 1. Nanotube contact used in nanotube conductance measurements. (**A**) Transmission electron micrograph of the end of a nanotube fiber recovered from the nanotube arc deposit. The fibers consist of carbon nanotubes and small graphitic particles. The fiber shown here is ~1 mm long and 0.05 mm at the tip, from which protrude several long and straight nanotubes. The nanotubes are very clean after they have been dipped in liquid metal (like the one shown), in contrast to the virgin tips on which many small graphitic particles are seen. The long nanotube is 2.2 μm long and 14 nm wide. The inset shows the end of the longest tube under higher magnification; it is bundled together with another one that terminates 400 nm before the first one. (**B**) Schematic diagram of the experimental setup. The nanotube contact is lowered under SPM control to a liquid metal surface. After contact is established, the current *I* is measured as the fiber is moved into the liquid metal, so that the conductance can be determined as a function of the position of the nanotube contact.

S. Frank, P. Poncharal, W. A. de Heer, School of Physics, Georgia Institute of Technology, Atlanta GA 30332, USA. Z. L. Wang, School of Materials Science and Engineering, Georgia Institute of Technology, Atlanta GA 30332, USA.

*To whom correspondence should be addressed.

nanotubes were completely free of particles.

In a typical experiment, the nanotube contact was lowered toward the liquid metal contact (LMC) with the coarse drive of the SPM. After electrical contact was established, the nanotube contact was cyclically driven in and out of the LMC under piezo control (peak-to-peak amplitude H_{pp} = 0.1 to 7 μm, frequency f = 0.1 to 10 Hz). A potential V_{ap} ~ 10 to 50 mV was applied to the contact, and the current through the circuit was measured together with the piezo displacement. Data from sequences of typically 200 to 1000 dipping cycles with 50,000 measured points per cycle were recorded automatically in each data file.

Figure 2A is a plot of conductance versus time for two time intervals in one sequence. The tip speed was ±5 μm/s. Each conductance cycle corresponds to one piezo cycle. The plateau at $1G_0$ indicates that the conductance of the contacting nanotube jumps from 0 to ~$1G_0$, where it remains constant for a time corresponding to a distance of ~2 μm along the nanotube. The constant value of the conductance is consistent with a ballistic conductor of uniform width and inconsistent with classical conductors for which the conductance varies as the inverse of the length. The observation of this ballistic property with a conductance near G_0 strongly suggests that this nanotube is indeed a quantized conductor. The abundance of corroborating experimental evidence, of which we present a representative sample here, verifies this property in general.

Usually we observed a sequence of steps at $1G_0$ intervals rather than a single step. These steps occur when other tubes also come into contact with the LMC, as in Fig. 2C, where a second step occurred after a dipping distance of 200 nm. This distance is consistent with the expected location of a second tube that is bundled together with the first (compare with inset, Fig. 1A). When the nanotube contact was submerged further, more nanotubes came into contact with the LMC and produced additional steps toward higher conductance, such as the step at 500 nm in Fig. 2C. Ultimately, the fiber touched the LMC and the residual resistance was on the order of 50 ohms (or <0.5% of the typical resistance of one nanotube).

In Fig. 2C, the conductance does not immediately rise to G_0 but is ~$0.5G_0$ for the first 25 nm. The major step at 200 nm is also preceded by an initial step ~40 nm long. This effect is frequently observed and can be related to the tip structure of the nanotubes (*23*–*26*). We found that ~30% of the nanotubes have tapered tips (*23*) that are up to twice as long as the diameter of the corresponding tube (Fig. 3B). This size is consistent with the lengths of the minor steps. The reduced conductance is readily explained in terms of the tip-to-shaft interface (*26*), which [like defects (*1*, *5*)] can elastically scatter electrons, thereby reducing the transmission coefficient (*21*, *22*) [see also (*19*)]. A close-up view of the tip effect is shown in Fig. 2D, where the scanning range was reduced to 70 nm. The pre-step at $G \approx \frac{1}{2}G_0$ is 34 nm long. The two well-defined peaks in the histogram of the corresponding sequence of 1000 traces are shown in Fig. 3A and indicate the reproducibility of this feature.

Complementary to the conductance traces, the data are also presented as conductance histograms (that is, the histogram of all the measured conductance points in a sequence) in order to average out noise and fluctuations. Figure 2B shows the histogram (actually plotted sideways) of 250 traces of Fig. 2A. The plateau near G_0 in Fig. 2A is represented by the peak in the histogram, which has a maximum that is very close to $1G_0$. The quantization is clear and is even more pronounced than in metal contacts. Moreover, we did not adjust for a "series contact resistor," as is often done for metal nanowires to align the conductance plateaus with conductance quanta (*16*–*19*).

Conductance quantization, as described here, was observed in all 20 nanotube contacts we constructed. However, in several cases, long anomalous plateaus (>500 nm)

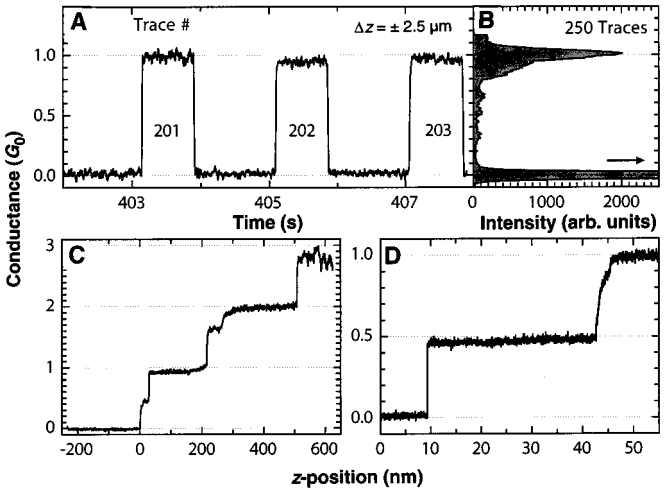

Fig. 2. Carbon nanotube conductance measurements. (**A**) Conductance of a nanotube contact that is moved at constant speed into and out of the mercury contact as a function of time. The period of motion is 2 s and the displacement Δz = ±2.5 μm. The conductance "jumps" to ~$1G_0$ and then remains constant for ~2 μm of its dipping depth. The direction of motion is then reversed and the contact is broken after 2 μm. The cycle is repeated to show its reproducibility; cycles 201 through 203 are displayed as an example. (**B**) Histogram of the conductance data of all 250 traces in the sequence. The plateaus at $1G_0$ and at 0 produce peaks in the histogram. The relative areas under the peaks correspond to the relative plateau lengths. Because the total displacement is known, the plateau lengths can be accurately determined; in this case, the $1G_0$ plateau corresponds to a displacement of 1880 nm. Plateau lengths thus determined are insensitive to random oscillations of the liquid level and hence are more accurate than measurements from individual traces. (**C**) A trace of a nanotube contact with two major plateaus, each with a minor pre-step. This trace is interpreted as resulting from a nanotube that is bundled with a second one (as in Fig. 1A, inset). The second tube comes into contact with the metal ~200 nm after the first. Shorter plateaus (from ~10 to 50 nm long) with noninteger conductance are often seen and are interpreted to result from the nanotube tips. A clear example of this effect is shown in (**D**).

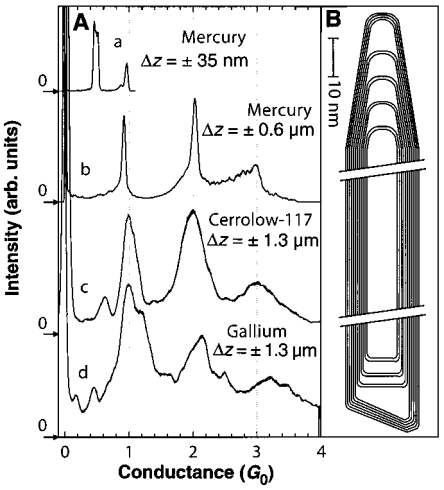

Fig. 3. (**A**) Nanotube histograms of nanotube contacts in various liquid metals. (a) Histogram of a nanotube (Δz = ±35 nm) in Hg. From the peak area, the tip length (corresponding to $G \approx \frac{1}{2}G_0$) is found to be 34 nm long, followed by a shaft for which $G \approx 1G_0$. (b) Histogram showing two distinct peaks at $0.9G_0$ and $2.05G_0$ with lengths of 159 and 339 nm, followed by a less distinct peak near $3G_0$ with a length of ~240 nm. (c) Nanotube contact histogram in liquid Cerrolow, showing a peak corresponding to a conductance plateau at $1G_0$ (length 530 nm), one at $2G_0$ (length 750 nm), and one at $3G_0$ (length 420 nm). (d) A histogram using liquid gallium with a peak at $1G_0$ (660 nm), one at $2G_0$ (520 nm), and a broader structure at $3.1G_0$ (370 nm). The broadened peak structures in (c) and (d) are caused by higher noise levels in these measurements. (**B**) Schematic diagram of a carbon nanotube (composed after high-resolution electron micrographs), showing two typical tip structures and a shaft. The tube is ~15 nm wide and is composed of 12 layers; the upper tip is 30 nm and the lower tip is ~7 nm long.

with $G \approx 0.5G_0$ were seen, although they always made steps close to $1G_0$. This effect could be caused by a defect in the tube whereby the transmission is reduced (*1, 5, 19*). Once the defect is pushed below the liquid metal level, its effect is "shorted out" and the conductance jumps to $1G_0$. However, we have never observed initial steps of $2G_0$ or greater.

We also performed similar measurements after replacing mercury with molten gallium and Cerrolow-117 (*28, 29*) (a lead-bismuth alloy) by heating the copper cup to 50° and 70°C, respectively. Precautions were taken to inhibit the oxidation of the metal surface. In all important aspects, the results were equivalent to those of the mercury experiments. Histograms of nanotube traces in all three metals are shown in Fig. 3. Aside from an increase in the peak width (which resulted from higher noise levels), the structure is similar to the Hg experiments. The conductance traces are also similar, with well-defined plateaus. This result indicates that the type of liquid metal used in the LMC does not affect the properties reported here. Again, small structures between the main peaks were observed, which arose from presteps of ~25 nm (that is, due to the tips).

The current-voltage characteristics of all samples were also recorded. The conductance of the nanotubes rose approximately linearly with applied voltage in the range $0.1\ V \leq |V_{ap}| \leq 2\ V$ and was approximately symmetric with respect to voltage polarity, although some anomalies have been observed (*30*). The rate of conductance change is $dG/dV \approx 0.5G_0$ per volt. The measurements reported above were all performed at low voltages ($V_{ap} \leq 50$ mV) so that the error due to this effect (a shift toward increased conductance) is small.

The nanotubes were not damaged even at relatively high voltages ($V_{ap} = 6$ V) for extended times, which corresponds to current densities $J > 10^7$ A cm^{-2} (for comparison, J for superconductors is typically on the order of 10^5 A cm^{-2}). This observation is remarkable because the power dissipated is 3 mW. If we assume that this power is dissipated uniformly along the length of the nanotube and assume a bulk thermal conductivity of 10 W cm^{-1} K^{-1}, then the middle of a nanotube 1 μm long and 20 nm in diameter would attain a temperature $T_{max} = 20{,}000$ K. This is clearly not possible (nanotubes start to burn at ~700°C), indicating that most if not all of the power must be dissipated elsewhere. In ballistic transport, heat is dissipated in the leads to the ballistic element and not in the element itself. Thus, our results indicate that electronic transport in the nanotubes is ballistic.

Recall that a conductance of $2G_0$ independent of diameter and length has been predicted for SWNTs (*5–7*). It has been further suggested that the conductance of MWNTs should scale with the number of layers (*7*). Consequently, for our tubes, which typically have 5 to 30 layers (*25*), one would expect conductance values in the range $10G_0 < G < 60G_0$, contrary to our finding of $G \approx 1G_0$.

The low measured conductance could indicate that only one layer contributes. Because SWNTs are semimetallic or metallic only when the helicity (m,n) is such that ($m - n$) is a multiple of 3 (*5, 6, 31–33*), only one-third of the layers of a MWNT should conduct; the others are larger gap (insulating) semiconductors. Because topologically the layers in a MWNT resemble a Russian doll (see Fig. 3B), each layer is closed and disconnected from every other. Hence, for a MWNT to conduct, the top layer must be conducting. If the next-to-top layer is insulating, then it and the deeper layers will not contribute to the conductance. Perhaps a conducting layer is usually followed by a nonconducting one because of geometrical and energy considerations, which impose conditions on layer-to-layer helicity changes and hence on the conductance properties.

Alternatively, the outer layer may be the only one to participate because the resistivity perpendicular to the tube axis is very high and consequently the layers are effectively insulated from each other. Note that in graphite, the *c*-axis resistivity ρ_c is very sensitive to defects: Increasing the defect density will decrease the interlayer resistivity. In natural graphite crystals, ρ_c ranges from $\sim 10^{-3}$ ohm·cm for imperfect crystals to >10 ohm·cm for the best natural ones (and even these are not defect-free) (*31*). Correspondingly, for a nanotube 1 μm long and 10 nm in diameter, the interlayer resistance (assuming $\rho_c = 10$ ohm·cm) would be ~1 kilohm, which is an order of magnitude smaller than a resistance quantum. However, our arc-produced nanotubes may be structurally almost perfect and ρ_c may be much greater than in natural crystals (*34*). In that case, only the outer layer contributes to the conductance. (Our tubes have not been subjected to ultrasound, chemical cleaning, or other potentially damaging procedures such as lithographically connecting them to solid metal leads.)

It remains to be explained why we observed a conductance of $1G_0$ rather than the expected $2G_0$ in our MWNTs. Perhaps the spin couples to the helicity (which can be represented by an axial vector), thereby resolving the spin degeneracy and halving the conductance in much the same way that a magnetic field lifts the spin degeneracy. Alternatively, it is possible that the framework of extrapolating the transport properties of MWNTs from SWNTs is oversimplified. Possibly, as for graphite, descriptions of the electronic transport properties require careful consideration of the interlayer interactions (*33*).

REFERENCES AND NOTES

1. L. Chico *et al*., *Phys. Rev. Lett.* **76**, 971 (1996).
2. W. A. de Heer, A. Châtelain, D. Ugarte, *Science* **270**, 1179 (1995).
3. M. Bockrath *et al*., *ibid.* **275**, 1922 (1997).
4. S. J. Tans *et al*., *Nature* **386**, 474 (1997).
5. L. Chico, L. X. Benedict, S. G. Louie, M. L. Cohen, *Phys. Rev. B* **54**, 2600 (1996).
6. W. Tian and S. Datta, *ibid.* **49**, 5097 (1994).
7. M. F. Lin and K. W.-K. Shung, *ibid.* **51**, 7592 (1995).
8. H. Dai, E. W. Wong, C. M. Lieber, *Science* **272**, 523 (1996).
9. L. Langer *et al*., *J. Mater. Res.* **9**, 927 (1994).
10. T. W. Ebbesen *et al*., *Nature* **382**, 54 (1996).
11. J. W. G. Wildoer, L. C. Venema, A. G. Rinzler, R. E. Smalley, C. Dekker, *ibid.* **391**, 59 (1998).
12. T. W. Odom, J.-L. Huang, P. Kim, C. M. Lieber, *ibid*., p. 62.
13. Earlier indications for quantization in carbon nanotubes were reported by W. A. de Heer and D. Ugarte, in *Nanowires,* P. A. Serena and N. Garcia, Eds. (NATO ASI Series E, Kluwer, Dordrecht, Netherlands, 1997), vol. 340, p. 227.
14. U. Landman, W. D. Luedtke, N. A. Burnham, R. J. Colton, *Science* **248**, 454 (1990); J. I. Pascual *et al*., *ibid.* **267**, 1793 (1995).
15. B. J. van Wees *et al*., *Phys. Rev. Lett.* **60**, 848 (1988).
16. J. I. Pascual *et al*., *ibid.* **71**, 1852 (1993).
17. D. P. E. Smith, *Science* **269**, 371 (1995).
18. M. Brandbyge *et al*., *Phys. Rev. B* **52**, 8499 (1995).
19. W. A. de Heer, S. Frank, D. Ugarte, *Z. Phys. B* **104**, 468 (1997).
20. S. Datta, *Electronic Transport Properties in Mesoscopic Systems* (Cambridge Univ. Press, Cambridge, 1995).
21. R. Landauer, *J. Phys. Cond. Matter* **1**, 8099 (1989).
22. _____, *Philos. Mag.* **21**, 863 (1970).
23. S. Iijima, *Nature* **354**, 56 (1991).
24. T. W. Ebbesen and P. M. Ajayan, *ibid.* **358**, 220 (1992).
25. D. Ugarte, A. Châtelain, W. A. de Heer, *Science* **274**, 1897 (1996).
26. D. L. Carroll *et al*., *Phys. Rev. Lett.* **78**, 2811 (1997).
27. Autoprobe CP (Park Scientific Instruments, Sunnyvale, CA).
28. None of the metals we used wets carbon nanotubes, although some of their oxides do [E. Dujardin, T. W. Ebbesen, H. Hiura, K. Tanigaki, *Science* **265**, 1850 (1994)].
29. Cerrolow-117 (Cerro Metal Products, Bellefonte, PA) is 44.7% Bi, 22.6% Pb, 8.3% Sn, 5.3% Cd, and 19.1% In.
30. S. Frank, P. Poncharal, Z. L. Wang, W. A. de Heer, in preparation.
31. M. S. Dresselhaus, G. Dresselhaus, P. C. Eklund, *Science of Fullerenes and Carbon Nanotubes* (Academic Press, San Diego, CA, 1996).
32. W. Mintmire, B. I. Dunlap, C. T. White, *Phys. Rev. Lett.* **68**, 631 (1992).
33. N. B. Brandt, S. M. Chudinov, Ya. G. Ponomarev, *Semimetals 1, Graphite and Its Compounds,* vol. 20.1 of *Modern Problems in Condensed Matter Science* (North-Holland, Amsterdam, 1988), pp. 74–77.
34. Indirect evidence for the purity and structural perfection comes from electron spin resonance measurements [O. Chauvet *et al*., *Phys. Rev. B* **53**, 13996 (1996)]; furthermore, the straightness is an indicator of structural perfection, because defects tend to bend the tubes [see (*8*)].

35. We thank U. Landman, R. L. Whetten, D. Ugarte, and P. First for helpful discussions. S.F. thanks the Alexander von Humboldt Foundation for financial support. Supported in part by the Army Research Office (grant DAAG 55-97-0133) and in part by the Georgia Tech Foundation.

6 March 1998; accepted 24 April 1998